Metals

Sintering aluminum alloy powder using direct current electric fields at room temperature in seconds

Brandon McWilliams[1,*], Jian Yu[1], and Frank Kellogg[2]

[1] U.S. Army Research Laboratory, Weapons and Materials Research Directorate, Aberdeen Proving Ground, MD 21005, USA
[2] SURVICE Engineering, Belcamp, MD 21017, USA

ABSTRACT

The sintering of a metallic alloy powder into bulk form using only direct current (DC) electric energy input at ambient room temperature is presented for the first time. It was found that a flash sintering phenomena is achievable in aluminum alloy powder, with no addition of external thermal energy, at applied DC electric fields in the range of 175–330 V/cm in which the formation of inter-particle necks occurs rapidly and is characterized by a near-instant change in the physical properties of the compact from electrically non-conductive to electrically conducting in a time period on the order of seconds. It was found that the kinetics of this effect have a logarithmic dependence on the magnitude of the applied electric field. Above approximately 330 V/cm, the critical field strength is reached at which an incubation time for flash sintering is not required and sintering occurs instantly with the application of the DC field. This technique has promise to greatly reduce processing time and costs associated with sintering of powder metallurgy products as well as consolidation of nanostructured metals by limiting exposure to high temperatures which result in excessive grain growth.

Introduction

Industrial powder metallurgy operations, such as press and sinter and hot pressing, require exposure to high temperatures for extended periods of time, which generally results in significant grain growth and a loss of the benefit of the initial microstructure of the feedstock material when processing nanostructured materials into bulk form [1]. In order to process novel nanocrystalline alloys with unique properties, e.g., high-temperature creep resistance

[2], it is necessary to explore other methods of consolidating metallic powders into fully dense form with minimal thermal energy input to preserve the initial microstructure of the feedstock. Alternative sintering techniques using electric fields in addition to thermal energy have been explored to enhance the kinetics of sintering by attempting to lower the activation energy required for the formation of inter-particle necks and subsequent densification. For example, spark plasma sintering (SPS) has successfully been utilized to consolidate conventional grain

Address correspondence to E-mail: brandon.a.mcwilliams.civ@mail.mil

size and nanocrystalline aluminum alloy powders which retain the grain size of the feedstock [3–7]. While the benefits of retaining nanocrystalline microstructure have been successfully demonstrated, the downfalls of this processing technique include [8]: high capital cost, batch processing and complex thermal–electric gradients within the compact resulting in non-uniform material properties [9, 10].

More recently, flash sintering, as reported by Raj and coauthors [11], has been widely used in ceramics research to rapidly (order of seconds) consolidate ceramic powders using DC fields. The flash sintering process uses larger electric fields (typically 100–1000 V/cm) and lower current densities (order of 100 mA/mm^2) than SPS-type processes. Flash sintering is characterized by a near-instant change in physical properties of the green body being sintered from non-conductive to conductive, as well as a discontinuous change in volume associated with densification due to sintering. Recent work in flash sintering of ceramics has shown that materials could be fully sintered at greatly reduced temperatures down to room temperature by using modified atmospheres containing hydrogen [12] or water [13], which is roughly an order of magnitude lower in temperature than which these materials can traditionally be processed.

The flash sintering phenomena was recently reported for aluminum alloy AA5083 powder by the authors [14] and is the first such report of flash sintering of metallic powders. It has been widely reported in the ceramics literature that increasing field strength decreases the activation energy for the flash to occur [11, 13]. The previously published results on AA5083 were consistent with this trend and it was shown that the temperature required to initiate the flash effect in AA5083 could be reduced from 403 to 306 °C by increasing the applied electric field strength from 28 to 56 V/cm [14]. In the present work, the flash sintering process with DC electric fields ranging from 150 to 330 V/cm is used to determine the feasibility of sintering AA5083 to near full density at room temperature.

Experimental methods

Commercial aluminum–magnesium alloy AA5083 (4.3 Mg–0.7Mn–0.15Cr, balance Al) gas atomized powder from Valimet, Inc. (Stockton, CA) was used in this study. The powder was sieved using − 325 mesh to give a starting powder with 98% of the particles with diameters of less than 45 μm and a mean average particle size of 11 μm. The powder was cold isostatically pressed (CIP) with an applied pressure of 140 MPa to form a master green compact. The morphology of the powder and the green compact were observed using scanning electron microscopy (SEM, Hitachi 4600) and are shown in Fig. 1. The micrograph of the green compact is representative of a fracture surface since the specimens were quite fragile and were not able to be polished metallographically. The morphology of the particles appears similar pre- and post-compaction indicating that the CIP process did not result in significant plastic deformation of the particles. The resulting green compact had a green density of 81% of the theoretical density of 2.66 g/cm^3 [15]. Rectangular specimens were sectioned from the master compact with dimensions of 10 × 10 × 3 mm for the following sintering experiments.

In the sintering experiments, the green pressed specimen is positioned between parallel copper electrodes which are connected to a DC power supply (Fig. 2). The DC power supply was operated in voltage control with limit set to give desired electric fields across the thickness of the specimen ranging from 150 to 330 V/cm. The initial conductivity of the green bodies was 2.5 MΩ m [14] which resulted in no observable current with a 1 mA lower detection limit on the power supply. As sintering progressed, the power supply was automatically switched to current control when (if) the specimen became conductive with a maximum of 3 A. The time progression of the experiment is shown schematically in Fig. 3. Real values were not plotted as voltage and current measurements were not acquired at high enough frequency in the flash regime to be representative and may be misleading to the reader if presented. All experiments were conducted at room temperature (T_{ambient} = 24 °C) with no externally applied heating. An infrared (IR) thermal imager (FLIR T460) was used with an acquisition interval of 1 s to observe any local thermal gradients and to quantify Joule heating of the specimen during the sintering process.

Figure 1 SEM micrographs of AA5083 powder pre-compaction (**a**) and green compact CIP to 140 MPa (**b**).
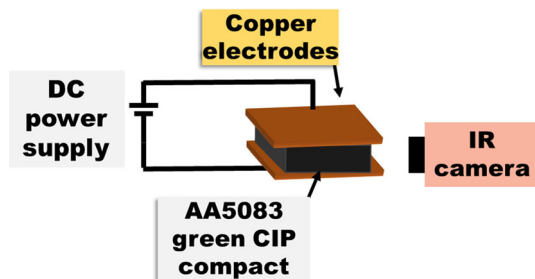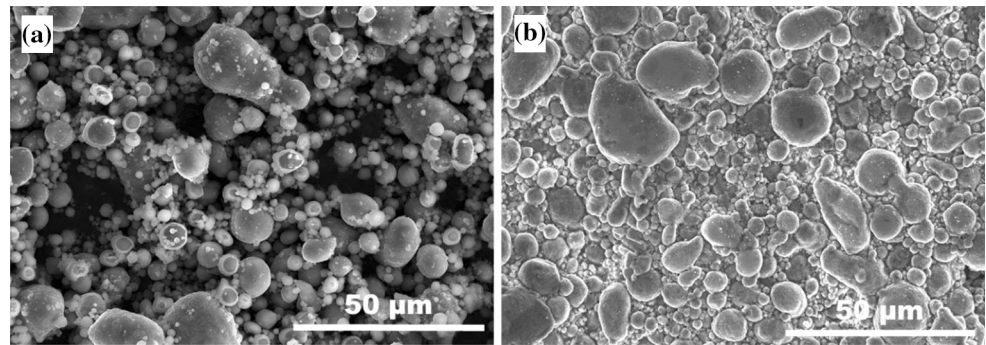
Figure 2 Schematic of experimental flash sintering system.
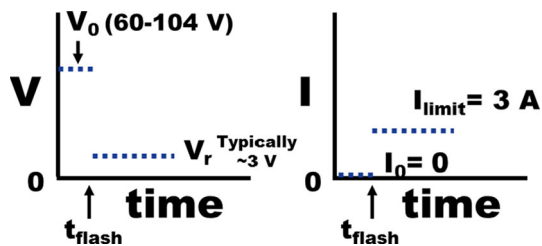
Figure 3 Schematic of flash sintering voltage and current versus time profiles. The sample is initially non-conductive and the DC power supply is in voltage control. At the flash point, the compact becomes conductive and the power supply is switched to current control with a 3 A limit, and the residual voltage (V_r) corresponds to the resistance of the specimen.

Following sintering, specimens were metallographically prepared for microstructure analysis using SEM and Vickers microhardness testing.

Results and discussion

All specimens, with the exception of the sample processed using a field of 150 V/cm, exhibited the flash sintering behavior in which the sample rapidly (order of seconds or less) transitioned from electrically insulating in behavior to electrically conducting and the power supply switched from voltage to current control. During this period, the peak current density was 27 mA/mm^2, which is calculated from the maximum current divided by the cross-sectional area of the specimen. In all experiments where a flash event was noted, thermal imaging revealed that sintering was confined to a relatively local region of approximately one quarter (or less) of the specimen. The resistivities of the specimens were calculated from the residual voltage after the power supply switched to current control with a 3 A limit. The resistivity of all samples ranged from 0.3 to 0.5 Ω m which is seven orders of magnitude lower than the green compact (2.5 MΩ m) which is indicative of a major change in microstructure. Figure 4 presents the temperature and heating rate histories at the location where maximum heating occurred, as well as thermal images at times before and after the flash event illustrating the localization of Joule heating. The flash time is defined as the time at which the peak heating rate is achieved and corresponds to $t = 660$ s in Fig. 4. While the maximum Joule heating is confined to regions where the microstructure has changed, i.e., interparticle necks have formed resulting paths for current to conduct [16], the rest of the sample is heated to a lesser extent through conduction from the local heat generation as can be observed in the thermal image at $t = 734$ s in Fig. 4. The maximum observable temperatures attained because of Joule heating in all tests varied greatly and ranged from 150 to 250 °C and did not have any correlation with applied electric field strength. The maximum temperature seemed more indicative of how much volume of material had sintered and the effect of the microstructure change on the local resistance and corresponding change in power dissipation through Joule heating.

Runaway Joule heating is often used to explain the mechanism for rapid mass transfer and enhanced kinetics observed during flash sintering [17, 18]. The

Figure 4 Temperature history during DC sintering experiment with applied electric field of 205 V/cm. History taken at location where maximum heating occurred. Inset thermal images show thermal gradients within the sample before and after the flash event at $t = 660$ s.
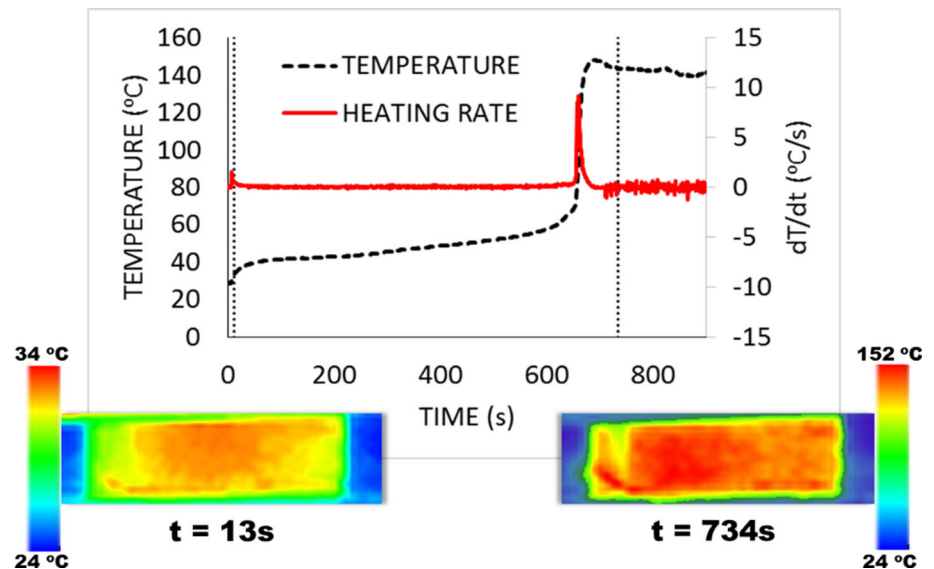

maximum temperature of 250 °C observed in the present experiments while sintering using DC fields and electric current is well below where sintering would traditionally be expected to be kinetically favorable for this alloy even when sintering under applied pressures (pressure increases sintering kinetics further) [7, 19]. References for pressureless sintering of this alloy were not found. This result suggests that the electric field contributes to reduce the thermodynamic free energy of the system and increases sintering kinetics. However, before conclusions can be drawn on whether or not it is indeed an electric field contribution to the sintering kinetics, it is important to note that these are surface temperature measurements and local heating occurring at particle contacts may be much higher [17, 18]. Prior analysis [20] on Joule heating at metallic particle contacts concluded that the local temperature increase at the contacts is likely to be insignificant for current densities in the range of 5–10 A/mm^2 which is several orders of magnitude larger than the current densities (0.027 A/mm^2) presently under investigation. Indeed, no evidence of melting was observed in posttest examination of the microstructure so it can be concluded that the local temperature did not exceed an upper bound of the solidus temperature of the alloy of 574 °C [15]. Based on this evidence, it is likely that the sintering kinetics observed presently are indeed the result of an electric field effect. The exact mechanisms for the field enhancement(s) are still under investigation and dielectric breakdown of

oxide layers on the surface of the particles may play a significant role [14].

Figure 4 also shows that there is a monotonic increase in temperature up to the time at which the flash event occurs. During this period, referred to in flash sintering literature as the incubation period [21], it is likely that there are a small number of conduction paths through the thickness of the sample resulting in Joule heating at the particle contacts, and appears to be relatively uniform across the width of the specimen (Fig. 4 inset $t = 13$ s). Other authors have concluded that high heating at these contacts results in local neck formation and the initial stages of sintering [17, 18]. As these necks continue to form and grow, the number of conduction paths monotonically increases and more current is able to flow resulting in additional Joule heating [22]. This process continues until a critical fraction of conduction paths is formed, at which point resistance is reduced by orders of magnitude and runaway Joule heating occurs, leading to rapid sintering of the remaining particles along the pathway.

Microstructural examination of polished samples from the sintered specimens revealed that in all cases where a flash event was observed neck formation and various degrees of sintering occurred (Fig. 5). In all cases, higher-density regions were found (Fig. 5a) where the highest temperatures were observed through thermal imaging, which supports the conclusion that conducting paths were formed through the formation of interparticle necks and densification of the green body. In other areas (Fig. 5b) of the
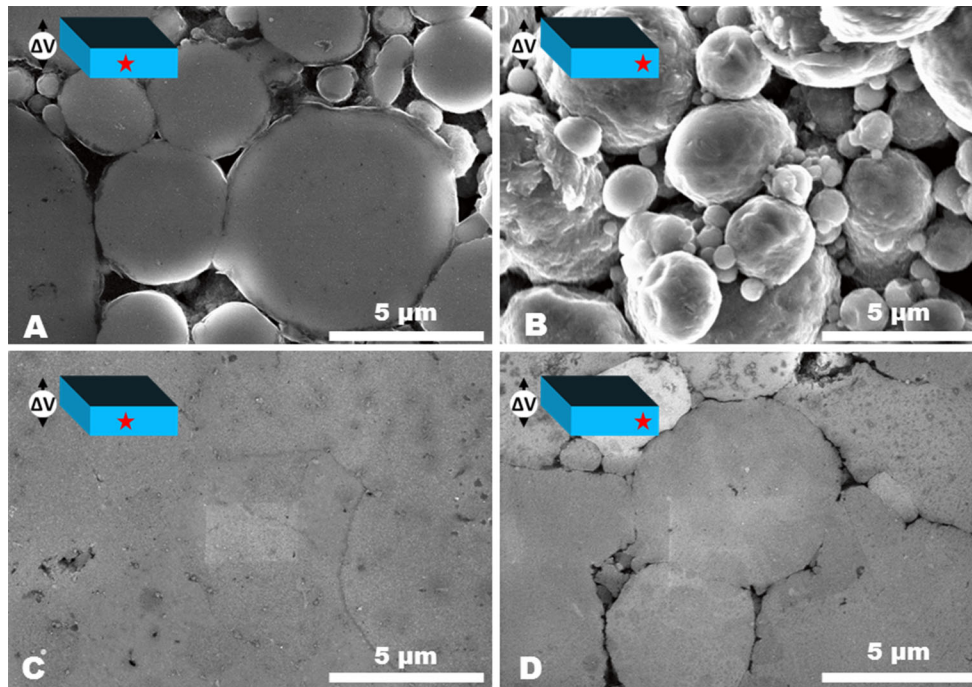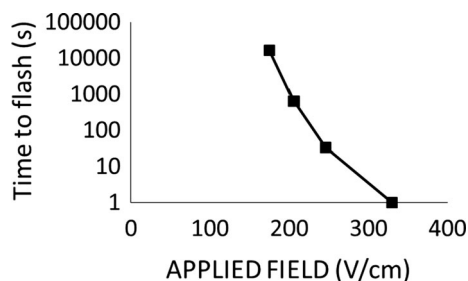
Figure 5 SEM micrographs of polished cross sections of samples sintered with 205 V/cm DC field showing: **a** formation of necks in sintered region of a specimen sintered once, **b** poorly sintered region of specimen sintered once, **c** near fully dense region of sample flashed multiple times in different orientations and **d** region of lowest density in sample flashed multiple times.

compact, the initial signs of neck formation can be observed, but very little densification could be observed.

Increasing the field strength had the effect of reducing the incubation time required for the flash event to occur. This result is consistent with the behavior observed during flash sintering of ceramics where it has been shown that increasing field strength generally increases the kinetics at which the flash occurs [11, 13, 18]. Figure 6 shows that this effect is logarithmic in nature for AA5083 over the range of DC field magnitudes studied presently. With an applied field of 330 V/cm, the specimen flash sintered instantly as the electric field was applied.

This indicates that 330 V/cm is above the critical field strength for which no incubation period is required for flash sintering to occur. The experiment with an applied field of 150 V/cm was terminated after holding for 12 h without observation of a flash, and posttest examination indicated no signs of sintering.

As all samples, regardless of applied field strength, were largely heterogeneous with only very localized regions of densification, an additional experiment was conducted to explore whether the apparent formation of favorable current/sintering paths could be controlled to activate additional critical pathways to produce a homogenously sintered specimen. In this final experiment, a sample was flash sintered, as detailed above, using a 205 V/cm field. While a larger field, e.g., 330 V/cm, would have reduced overall process time, the 205 V/cm voltage level was selected to give more time to observe the sample prior to flash. Based on the single-pass experiments presented previously, there are not any expected differences in microstructure if a voltage with faster flash incubation time was to be used to speed up the overall process. This sample behaved similarly to the specimens above and current did not pass through the sample prior to the flash time as shown schematically

Figure 6 Time until flash (logarithmic scale) event occurred after turning on electric field versus DC field strength.

Figure 7 Vickers microhardness map of sample flash sintered multiple times in different orientations (half of sample mapped), showing relative uniformity of properties.
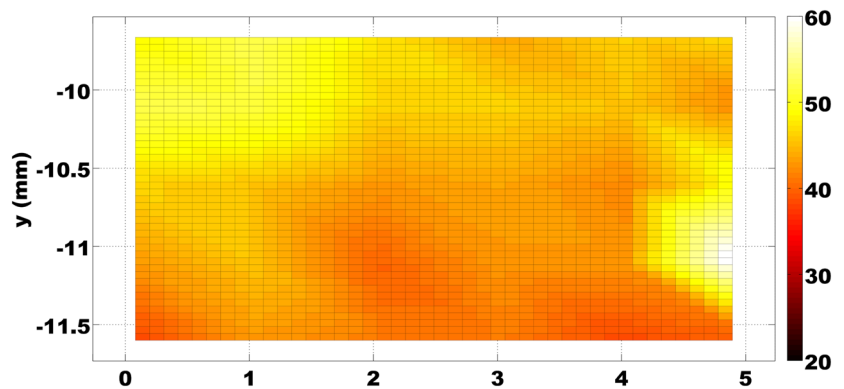
in Fig. 3. After the flash event occurred, the sample became electrically conducting and the current was maintained at the 3 A limit set by the power supply. The resistivity of the material was calculated from the voltage as 0.30 Ω m. The sample was then rotated 90° around the Z (thickness direction axis) and the experiment repeated. On the second pass, the sample was again initially non-conductive (i.e., $I_0 = 0$) in the new orientation and again became conducting after the second flash. This process was repeated until the sample had been flash sintered in all orientations (six total passes) of the rectangular prism-shaped compact. After all passes, the resistivity of the material did not vary much and was in the range of 0.28–0.30 Ω m. The sample was observed to be non-conducting (within the limits of our measurements) in all orientations in which the field was applied. This would imply a diode effect when sintering two orientations which are rotated 180° from one another which is not likely. It is possible that the physical and heterogeneous change in microstructure of the sample from preceding 90° rotations may have occurred in such a way that when the pass which corresponded to 180° of one of the three principal directions occurred, the previously formed percolation path for conduction had been disrupted. This phenomenon requires further exploration in future work.

The final resulting compact had a nearly uniform temperature distribution when an electric current was applied and microstructural examination revealed a much higher-density compact (Fig. 5c). The sample still had some heterogeneity, as shown in Fig. 5d, which is representative of the lowest density regions in the sample, but exhibit higher-density than the best regions in the single-pass specimen (Fig. 5a). The overall bulk density of the sample, as measured using Archimedes' method, for this sample was 90%

of theoretical. As evidenced by the micrographs in Fig. 5c, a large portion of the sample was much higher than 90%, and nearly fully dense, which gives positive indication that the method may be refined further to obtain bulk samples using this rapid processing technique, while minimizing exposure to elevated temperatures.

Vickers microhardness measurements were taken in a 1 × 1 mm grid on the sample flashed multiple times to generate the contour plot shown in Fig. 7. Microhardness measurements of the dense regions were obtained and averaged 39.5 HV with a standard deviation of 6.1 HV. Measurements were only able to be taken in the locally densified regions, so a contour of the hardness of the sample was able to be generated. The hardness of the multiple flashed samples is on average much higher than the single experimental specimen and has large regions that are 80% the hardness of wrought AA5083 [23]. The hardness measurements indicate that the properties of the sample are fairly homogenous across the cross section and it is expected that additional flash sintering passes could be used to increase density and uniformity even further.

Conclusions

In summary, it was demonstrated for the first time that a metallic alloy, aluminum alloy 5083, exhibits flash sintering behavior and was able to be consolidated at room temperature without the additional of any externally applied thermal energy. It was found that the kinetics of this effect have a logarithmic dependence on the magnitude of the applied electric field. Above approximately 330 V/cm, the critical field strength is reached at which an incubation time

for flash sintering is not required and sintering occurs instantly with the application of the DC field. The flash effect appears to depend on the development of favorable conduction paths through the thickness of the sample, which has a tendency to result in localized sintering behavior when a critical volume of interparticle necks forms locally. It was shown that manipulation and generation of additional conduction paths in a previously flash sintered specimen can be achieved through altering sample orientation and using multiple sintering passes. The results indicate that uniform and fully dense material can be obtained by sintering AA5083 with a DC electric field at room temperature. This technique has promise to greatly reduce processing time and costs associated with sintering of powder metallurgy products. Additionally, development of nanocrystalline metals with disruptive improvements in physical and mechanical properties has been limited by the ability to manufacture these materials into bulk form while retaining the microstructure due to the high temperatures required by traditional sintering processes. Flash sintering of these materials may prove a viable option to expedite the material development cycle and efficiently manufacture these materials into forms suitable for insertion to the marketplace.

Compliance with ethical standards

Conflict of interest The authors declare that they have no conflict of interest.

References

[1] Lavernia EJ, Han BQ, Schoenung JM (2008) Cryomilled nanostructured materials: processing and properties. Mater Sci Eng A 493(2008):207–214

[2] Darling KA, Rajagopalan M, Komarasamy M, Bhatia MA, Hornbuckle BC, Mishra RS, Solanki KN (2016) Extreme creep resistance in a microstructurally stable nanocrystalline alloy. Nature 537:378–381

[3] Ye J, Ajdelsztajn L, Schoenung JM (2006) Bulk nanocrystalline aluminum 5083 alloy fabricated by a novel technique: cryomilling and spark plasma sintering. Met Mater Trans A 37A:2569–2579

[4] Xiong Y, Liu D, Li Y, Zheng B, Haines C, Paras J, Martin D, Kapoor D, Lavernia EJ, Schoenung JM (2012) Spark plasma sintering of cryomilled nanocrystalline Al alloy-part I: microstructure evolution. Met Mater Trans A 43A:327–339

[5] Sasaki TT, Ohkubo T, Hono K (2009) Microstructure and mechanical properties of bulk nanocrystalline Al–Fe alloy processed by mechanical alloying and spark plasma sintering. Acta Mater 57:3529–3538

[6] Kellogg F, McWilliams B, Sietins J, Giri A, Cho K (2017) Comparison of SPS processing behavior between as atomized and cryomilled aluminum alloy 5083 powder. Met Mater Trans A 48A:5492–5499

[7] Kellogg F, McWilliams B, Cho K (2016) Effect of current pathways during spark plasma sintering of an aluminum alloy powder. Met Mater Trans A 47A:6353–6367

[8] Guillon O, Gonzalez-Julian J, Dargatz B, Kessel T, Schierning G, Rathel J, Herrmann M (2014) Field-assisted sintering technology/spark plasma sintering: mechanisms, materials, and technology developments. Adv Eng Mater 16:830–849

[9] Zavaliangos A, Zhang J, Krammer M, Groza JR (2004) Temperature evolution during field activated sintering. Mater Sci Eng A 379:218–228

[10] McWilliams B, Yu J, Zavaliangos A (2015) Fully coupled thermal-electric-sintering simulation of electric field assisted sintering of net-shape compacts. J Mater Sci 50:519–530. https://doi.org/10.1007/s10853-014-8463-1

[11] Cologna M, Rashkova B, Raj R (2010) Flash sintering of nanograin zirconia in < 5 s at 850 C. J Am Ceram Soc 93:3556–3559

[12] Zhang Y, Luo J (2015) Promoting the flash sintering of ZnO in reduced atmospheres to achieve nearly full densities at furnace temperatures of < 120 C. Scr Mater 106:26–29

[13] Nie J, Zhang Y, Chan JM, Huang R, Luo J (2018) Water-assisted flash sintering: flashing ZnO at room temperature to achieve ∼ 98% density in seconds. Scr Mater 142:79–82

[14] McWilliams B, Yu J, Kellogg F, Kilczewski S (2017) Enhanced sintering kinetics in aluminum alloy powder consolidated using DC electric fields. Met Mater Trans A 48(2017):919–929

[15] Hardesty F (ed) (1990) ASM handbook, volume 2: properties and selection: nonferrous alloys and special-purpose materials. ASM International, Metals Park, pp 62–122

[16] Olevsky E, Bogachev I, Maximenko A (2013) Spark-plasma sintering efficiency control by inter-particle contact area growth: a viewpoint. Scr Mater 69:112–116

[17] Zhang Y, Jung JI, Luo J (2015) Thermal runaway, flash sintering and asymmetrical microstructural development of ZnO and ZnO–Bi_2O_3 under direct currents. Acta Mater 94:87–100

[18] Todd RI, Zapata-Solvas E, Bonilla RS, Sneddon T, Wilshaw PR (2015) Electrical characteristics of flash sintering: thermal runaway of Joule heating. J Eur Ceram Soc 35:1865–1877

[19] Liu D, Xiong Y, Li P, Lin Y, Chen F, Zhang L, Schoenung JM, Lavernia EJ (2016) Microstructure and mechanical behavior of NS/UFG aluminum prepared by cryomilling and spark plasma sintering. J Alloys Compd 679:426–435

[20] Trapp J, Kieback B (2015) Temperature distribution in metallic powder particles during initial stage of field-activated sintering. J Am Ceram Soc 98:3547–3552

[21] Cologna M, Francis JSC, Raj R (2011) Field assisted and flash sintering of alumina and its relationship to conductivity and MgO-doping. J Eur Ceram Soc 31:2827–2837

[22] Zhang J, Zavaliangos A (2011) Discrete finite-element simulation of thermoelectric phenomena in spark plasma sintering. J Electron Mater 40:873–878

[23] Gale WF, Totemeier TC (2004) Smithells metals reference book. Elsevier Butterworth-Heinemann, Oxford